CHEMISTRY OF MATERIALS

ACS Editors' Choice

Article

pubs.acs.org/cm

Terms of Use

Iron-Loaded Magnetic Nanocapsules for pH-Triggered Drug Release and MRI Imaging

Hongyu Chen,[†,⊥] Dino Sulejmanovic,[†,#] Thomas Moore,[‡] Daniel C. Colvin,[§] Bin Qi,[∥] O. Thompson Mefford,[∥] John C. Gore,[§] Frank Alexis,[‡] Shiou-Jyh Hwu,[†] and Jeffrey N. Anker*[,†]

[†]Department of Chemistry, Center for Optical Materials Science and Engineering (COMSET), and Environmental Toxicology Program, Clemson University, Clemson, South Carolina 29634, United States

[‡]Department of Bioengineering, Clemson University, Clemson, South Carolina 29634, United States

[§]Vanderbilt University Medical Center, Vanderbilt University, Nashville, Tennessee 37232, United States

[∥]Department of Materials Science and Engineering and Center for Optical Materials Science and Engineering (COMSET), Clemson University, Clemson, South Carolina 29634, United States

Supporting Information

ABSTRACT: Magnetic nanocapsules were synthesized for controlled drug release, magnetically assisted delivery, and MRI imaging. These magnetic nanocapsules, consisting of a stable iron nanocore and a mesoporous silica shell, were synthesized by controlled encapsulation of ellipsoidal hematite in silica, partial etching of the hematite core in acid, and reduction of the core by hydrogen. The iron core provided a high saturation magnetization and was stable against oxidation for at least 6 months in air and 1 month in aqueous solution. The hollow space between the iron core and mesoporous silica shell was used to load anticancer drug and a T_1-weighted MRI contrast agent (Gd-DTPA). These multifunctional monodispersed magnetic "nanoeyes" were coated by multiple polyelectrolyte layers of biocompatible poly-L-lysine and sodium alginate to control the drug release as a function of pH. We studied pH-controlled release, magnetic hysteresis curves, and T_1/T_2 MRI contrast of the magnetic nanoeyes. They also served as MRI contrast agents with relaxivities of 8.6 mM^{-1} s^{-1} (r_1) and 285 mM^{-1} s^{-1} (r_2).

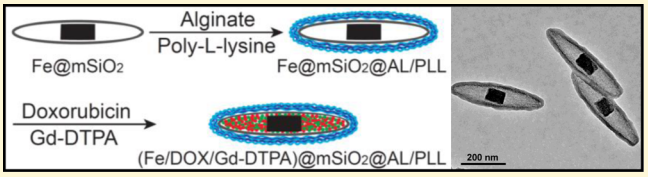

INTRODUCTION

Doxorubicin (DOX) is used as a chemotherapy drug to treat a wide range of cancers. However, its use is hindered by relatively low selectivity toward cancer cells and severe side effects from uptake by noncancerous cells and tissue.[1,2] Thus, targeted drug delivery systems are preferred to increase the efficiency of drug delivery to specific tissues as well as to decrease its side effects. Nanosized delivery system with a pH-responsive controlled release behavior could address this issue by releasing drugs into the blood only gradually but rapidly release drugs after endocytosis in acidic tumor lysosomes and endosomes. The particles could be targeted to tumors via enhanced permeability and retention (EPR) effect and by functionalizing the nanoparticle surface with appropriate antibodies or other targeting molecules.

As drug carriers, multifunctional magnetic nanomaterials have attracted broad interest because of their utility in biomedical applications such as drug delivery carriers,[3−7] magnetic resonance imaging (MRI),[8] bioseparation,[9] fluorescent labeling,[10,11] hyperthermia,[12] and immunoassays.[13] These magnetic nanomaterials have been also used for guided accumulation toward a target site with an external magnetic field.[14,15] So far, nanoparticles based on iron oxide are most commonly used as nanoparticle magnetic carriers because of their relatively high saturation magnatization and low-toxicity.[14,15] However, magnetic nanocarriers with stronger magnetization are still in urgent need for practical magnetic field-mediated drug delivery. Recently, iron nanoparticles or iron nanoparticles with iron oxide shells have also gained attention as MRI contrast agents due to their higher magnetization and stronger shortening effect on T_2 relaxation time than IONPs.[16−19] However, the T_1 weighed MRI relaxivity of these iron nanoparticles (r_1 = 1.2 $s^{-1}mM^{-1}$) is not as good as FDA-approved T_1 weighted contrast agents such as Gd-DTPA (r_1 = 6.2 $s^{-1}mM^{-1}$ measured at 1.5 T).[17] Hence, a nanosystem combining the advantages of both stable iron nanoparticles with high saturation magnetization and biocompatible polymeric layer for pH triggered drug release is expected to expedite the development of multifunctional delivery systems.

In 2010, Chen and co-workers reported a porous silica coated rattle type of particle (Fe_2O_3@$mSiO_2$) for magnetic field-mediated drug (DOX) delivery.[20] However, the DOX was encapsulated into the porous silica, which has limited drug loading volume and provides limited control of the sustained release process. Polyelectrolyte capsules composed of weak

Received: December 19, 2013
Revised: February 24, 2014
Published: February 26, 2014

polyelectrolytes are responsive to the pH of the environment. The mechanism of pH-triggered release from nanocarriers based on polyelectrolytes was well established based on previous reports.[21,22] In 2000, Mendelsohn et al. observed that pore formation occurs when a multilayer polyelectrolyte complex, composed of poly(styrene sulfonate)/poly(allylamine hydrochloride), is placed in an acidic environment, whereas the pores disappeared at a neutral environment.[23] In our previous study, PSS and PAH were used to create a pH-controlled release shell for DOX on radioluminescent hollow capsules.[24] Similar to PLL and AL, PSS and PAH are weak polyacid and polybase, respectively. However, uncoated PAH is cytotoxic at high concentrations. In order to create a biocompatible layer to control DOX release in our study, we coated the nanocapsules with poly-L-lysine (PLL) and sodium alginate (AL), which are widely used biocompatible polymers.[25,26]

Herein, we developed a novel and facile strategy to fabricate highly stable iron nanoparticles with a silica nanocapsule and biocompatible polymeric layer as nanocarriers for pH triggered release for anticancer drug (doxorubicin, DOX) and MRI imaging. These stable iron nanoparticles were for the first time used as anticancer drug carriers. In order to enhance the drug loading efficiency, a selective etching strategy was used to create a hollow space for drug loading. Multilayers of biocompatible polyelectrolytes were coated by layer-by-layer (LbL) technique on the surface of nanocarrers to control the drug release rate by pH. The LbL technique was introduced by Decher and Caruso.[27,28] This technique is recently developed to coat colloidal particles with polyelectrolytes based on electrostatic attraction.[29−32] The iron nanocores are good T_2-weighted contrast agents with high relaxivities. In order to realize dual MRI contrast imaging (T_1-weighted and T_2 weighted) to improve imaging specificity, an FDA-approved T_1 weighted contrast agent (Gd-DTPA) was encapsulated with DOX into our magnetic nanocarrier. These dual MRI-contrast nanocapsules are promising agents for locating and tracking the encapsulated drugs during magnetic drug delivery.

EXPERIMENTAL SECTION

Materials. Tetraethoxysilane (TEOS), poly-L-lysine (PLL, MW 15 000−30 000), cetyltrimethylammonium bromide (CTAB), Diethylenetriaminepentaacetic acid gadolinium(III) dihydrogen salt hydrate (Gd-DTPA), iron(III) chloride anhydrous, doxorubicin hydrochloride, sodium chloride, and potassium phosphate monobasic were purchased from Sigma-Aldrich (St. Louis, MO). Oxalic acid, ammonium hydroxide, sodium hydroxide, ethanol, and nitric acid were obtained from BDH Chemicals Ltd. (Poole, Dorset, U.K.). Deionized (DI) water was purchased from EMD Chemicals Inc. (Gibbstown, NJ, U.S.A.). Polyvinylpyrrolidone (PVP K-30, MW 40 000) was purchased from Spectrum Chemicals (Gardena, CA). Sodium alginate (AL, low viscosity) was obtained from Alfa Aesar. Agarose (low melting point) was purchased from Shelton Scientific (Peosta, IA). All chemicals were used as received without further purification.

Preparation of Monodispersed Mesoporous Silica Coated Hematite Nanorice (α-Fe_2O_3@SiO_2). Monodispersed spindle-shaped hematite nanotemplate with controllable aspect ratios were fabricated were prepared according to the method described by Ozaki and co-workers. Typically, 100 mL of aqueous solution containing 2.0 × 10^{-2} M $FeCl_3$ and 4.0 × 10^{-4} M KH_2PO_4 were aged at 100 °C for 72 h. The resulting precipitate was centrifuged and washed three times with water. The mesoporous silica shell was obtained according to the literature.[33] The spindle-shaped hematite particles, synthesized as above, were dispersed ultrasonically into a 80 mL solution containing CTAB (0.1 g), water (60 mL), and ethanol (60 mL). The suspension was stirred using a magnetic stir bar at room temperature and a solution of TEOS (150 μL) in 20 mL ethanol was added, followed by 2 mL of ammonia hydroxide. After 6 h, the reaction mixture was precipitated by centrifuging at 4000 rpm for 16 min. The particles were washed three times with ethanol and centrifuged to collect the product.

Preparation of Silica-Coated Magnetic Nanoeyes (Fe@SiO_2). To partially etch the hematite core, the above silica-encapsulated hematite nanoparticles were suspended in 180 mL distilled water with 1.8 g PVP and 11.34 g oxalic acid (0.5 M) and incubated at 60 °C for 10.5 h. The hematite partially dissolved particles were collected by centrifugation and rinsed with DI water twice. The obtained particles were dried at oven at 80 °C overnight. The CTAB template in the silica shell was removed by calcining the particle powder in a furnace at 600 °C for 6 h. This powder was then transferred to a tube furnace with ultrapure hydrogen (99.99%) flow at 525 °C for 4 h. The product was then naturally cooled to room temperature and gradually passivated with 1% O_2/Ar mixed gas. Finally, the spindle-shaped porous silica-coated iron nanoparticles were obtained.

Synthesis of Silica Nanoparticles Preparation for BJH Pore Size Determination. The preparation for mesoporous silica nanoparticles is similar to the silica shell coating on hematite nanorice. A mixed solution containing CTAB (0.1 g), water (60 mL), and ethanol (60 mL) was stirred using a magnetic stir bar at room temperature and a solution of TEOS (150 μL) in 20 mL ethanol was added, followed by 2 mL of ammonia hydroxide. After 6 h, the reaction mixture was precipitated by centrifuging at 4000 rpm for 16 min. The particles were washed three times with ethanol and centrifuged to collect the product. The CTAB template in the silica shell was removed by calcining.

Preparation of Biocompatible Polymer-Coated Magnetic Nanoeyes (Fe@SiO_2@PLL/AL) Loaded with DOX and Gd-DTPA. PLL solution (2 mL) with concentration of 5 mg mL^{-1} in 0.5 M NaCl was added to a 10 mL aqueous suspension (pH 6) of 60 mg magnetic nanoeyes (Fe@SiO_2). After ultrasonic treatment for 10 min, the suspension was collected by centrifugation and washed three times in distilled water. Gentle shaking followed by ultrasonic treatment for 1 min was used to disperse the particles after centrifugation. Then, the particles were resuspended in 10 mL aqueous solution (pH 8.0) with 2 mL oppositely charged AL (5 mg mL^{-1} in 0.5 M NaCl) and sonicated for 10 min. The PLL coating process was repeated for four times and the AL coating was repeated for another four times. Finally, a composite of biocompatible polymer coated with magnetic nanoeyes were obtained. The DOX was loaded into the biocompatible polymer coated magnetic nanoeyes by incubating DOX (20 mg) and Gd-DTPA (20 mg) with magnetic nanoeyes (20 mg) in 2 mL water (pH 5.0, adjusted by 1 mM HCl) at room temperature under vacuum. After the water completely evaporated, the free DOX was removed by repeated washing with water (pH 8.0, adjusted by 1 mM NaOH) until the supernatant was clear. The encapsulated amount of DOX or Gd-DTPA was calculated by subtracting the DOX or Gd-DTPA residue from the initially added amount of DOX or Gd-DTPA.

In Vitro pH-Triggered Release Study of DOX and Gd-DTPA. 200 μL of DOX and Gd-DTPA encapsulated nanocapsules with polyelectrolyte mutilayers (10 mg/mL) were suspended with release media at pH 5.0 and 7.4 in Slide-A-Lyzer MINI dialysis units at room temperature. The release medium was removed for analysis at given time intervals and replaced with the same volume of fresh release medium. The DOX concentration was measured with high performance liquid chromatography (HPLC) on a Waters system using an Alltima C18 column (250 × 4.6 mm, 5 μm). Gadolinium content in the release media was performed by inductively coupled plasma (ICP) (Optima 3100 RL, Perkin-Elmer).

Preparation of Nanocapsules for MR Imaging. T_1 and T_2 MRI measurements were acquired for the (Fe/DOX/Gd-DTPA)@SiO_2@PLL/AL particles at a series of concentrations. The particles were dispersed in 1% agarose gel at 80 °C and cooled to room temperature in NMR tubes to set the gel. The gel prevented settling and aggregation allowing MRI imaging several days after preparation.

Cell Viability Test. MCF-7 breast cancer cells were seeded at a density of 10 000 cells/well in a 96-well plate. Cells were stored at 37

°C at 5% CO_2 and attached to the plate overnight. Nanoparticles (iron core, silica shell, Fe@SiO_2, and Fe@SiO_2@PLL/AL) were suspended in media, sonicated for 10 min to disperse, and diluted to 1000, 500, 250, 100, and 50 μg/mL. Media was removed from wells and fresh media or nanoparticle in media was added to each well. Five repeats were done for each concentration. Nanoparticles were incubated with cells overnight and the next day a Presto Blue assay (Life Technologies) was performed. Media was removed and 100 μL of a 1:9 ratio Presto Blue in culture media was added to each well. Cells were incubated at 37 °C and 5% CO_2 for 45 min. Fluorescent intensity was measured with a plate reader with an excitation wavelength of 560 nm and an emission wavelength of 590 nm. Fluorescent intensity for each concentration of nanoparticle was normalized as a percentage of the fluorescent intensity of the control cells. Percent viability averages were plotted with error bars of one standard deviation. Cell viability of test of MCF-7 cells on free DOX, (Fe/DOX/Gd-DTPA)@SiO_2 nanocapsules, and (Fe/DOX/Gd-DTPA)@SiO_2@AL/PLL nanocapules at different DOX concentrations was performed in the same way after incubation for 48 h (with n = 6 replicate trials).

Characterization Methods. Transmission and scanning electron microscopy were performed on a H9500 operated at 300 kV and HD2000 microscope operated at 100 kV, respectively. An X-ray diffractometer (Rigaku; MiniFlex, Cu Kα) was used to characterize the XRD pattern of the prepared nanoparticles. Nanoparticle ζ-potential and hydrodynamic diameter was measured with a Zetasizer Nano ZS (equipped with a 633 nm He−Ne laser) from Malvern Instruments. Prior to the experiment, the particles were diluted in distilled water to 0.1 mg/mL. Magnetization measurements were performed at 300 K using vibrating sample magnetometer (VSM) option of physical property measurement system (PPMS, Quantum Design, U.S.A.), with the applied magnetic field sweeping between ±3.0 T at a rate of 50 Oe/sec. Determination of the iron and gadolinium content in a sample was performed by inductively coupled plasma (ICP) (Optima 3100 RL, Perkin-Elmer). Fourier transform infrared spectra (FTIR) were acquired with a Thermo-Nicolet Magna 550 FTIR instrument. The N_2 adsorption/desorption isotherm was measured at liquid nitrogen temperature (77 K) using a Micromeritics ASAP 2010 M instrument. The pore size distribution was obtained from the Barret−Joner−Halenda (BJH) method.[34] The fluorescence image of DOX-loaded nanocapsules in water (Supporting Information Figure S4) was taken on a Nikon microscope (Eclipse Ti, Nikon, Melville, NY) with a CCD camera (Nikon DS-2MBW), using 488 nm excitation and a 535 long-pass emission filter.

All MRI experiments were performed on a Varian 4.7 T horizontal bore imaging system (Agilent Inc., Santa Clara, CA). Samples, contained in 5 mm NMR tubes, were placed in a 63 mm inner diameter quadrature RF coil for imaging. MRI gradient echo scout images were collected in all three imaging planes (axial, coronal, and sagittal) for subsequent image planning, with repetition time (TR) = 100 ms, echo time (TE) = 4 ms, number of slices = 20, slice thickness = 2 mm, matrix size 128 × 128, field of view (FOV) = 40 mm × 40 mm, number of acquisitions (NEX) = 2. Relaxivity measurements were then collected on a single 2 mm thick imaging slice, approximately perpendicular to the long axis of the NMR tubes. T_2 relaxivity measurements were acquired with FOV = 36 mm × 36 mm, using a multispin echo imaging sequence with TR = 3000 ms, NEX = 10, echo spacing = 4 ms, number of echoes = 10, and 128 × 128 matrix. T_1 relaxivity measurements were acquired using the same slice geometry and imaging matrix with a segmented fast low angle shot (FLASH) sequence with inversion recovery with inversion times of 50, 97, 186, 360, 695, 1341, 2590, and 5000 ms, with TR = 6000 ms, TE = 2.1 ms, and NEX = 8.

Following data collection, images were analyzed using Matlab 2011a (The Mathworks, Inc., Natick, MA). Regions of interest (ROIs), encompassing approximately 70−80 voxels, were manually drawn in each sample, and the signals from those voxels averaged to obtain a mean signal for each sample. The same ROI was used to calculate the mean signal of the sample across all echo times.

RESULTS AND DISCUSSION

Previous studies on particle shape showed that particles (>500 nm in length) with high aspect ratio have a slower clearance rate than particles with low aspect ratio (e.g., spherical particles) for drug delivery systems.[35−38] Iron oxide nanoparticles with high aspect ratio were chosen as templates to synthesize monodispersed magnetic nanocapsules. This technique is highly flexible for controlling the nanocapsule size and shape by varying the synthesis condition of template of iron oxide nanoparticles.[24,39−43] The length of these nanocapsules can be tuned from 20 to 600 nm and the aspect ratio can be adjusted from spheres to prolate spheroids depends on the prepared templates. In order to obtain monodispersed magnetic nanocapsules, as shown in Figure 1A, monodispersed

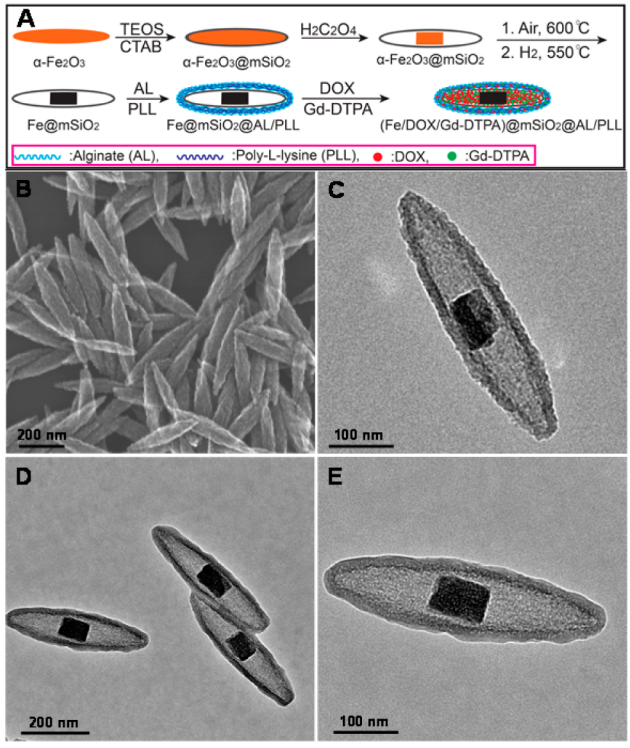

Figure 1. (A) Schematic showing the synthesis route of sodium alginate and poly-L-lysine coated nanoeye for pH triggered drug release, (B) SEM image of α-Fe_2O_3 nanorice, (C) TEM image of silica coated iron nanoeyes (Fe@SiO_2), (D) TEM image of sodium alginate and poly-L-lysine coated Fe@SiO_2 nanoparticles (Fe@SiO_2@AL/PLL) in low magnification, (E) TEM image of sodium alginate and poly-L-lysine coated Fe@SiO_2 nanoparticles (Fe@SiO_2@AL/PLL) in high magnification.

hematite nanorice was prepared first, then treated through a modified Stöber procedure to form a mesoporous silica shell with the assistance of CTAB.[44] Finally the hematite core was partially dissolved by etching in 0.5 M oxalic acid for 10.5 h according to our early work on the selective etching.[43] Unlike our early work on the Fe_3O_4 based nanoparticle synthesis by using 5% hydrogen (H_2/N_2),[43] ultrahigh pure hydrogen (99.99%) was used to convert the hematite nanocore into iron nanocore at 525 °C for 4 h. Without the mesoporous silica coating, irreversible aggregation of the iron cores was found during the hydrogen reduction (Figure S1, Supporting Information). In order to stabilize the iron nanoparticles for biological applications, the surface of iron nanoparticles was

dx.doi.org/10.1021/cm404168a | Chem. Mater. 2014, 26, 2105−2112

passivized by 1% oxygen (O_2/Ar) at room temperature. To apply these magnetic nanoeyes for pH triggered drug release, multilayers of biocompatible polyelectrolytes (four layers of positively charged poly-L-lysine and four layers of negatively charged sodium alginate) were then alternately coated onto the negative charged (−18.5 mV) silica coated iron nanoparticles (Fe@SiO_2).

The SEM image in Figure 1B shows monodispersed spindle-shaped hematite nanorice. Figure 1C represents the intact silica shell after the iron oxide core was partially dissolved by oxalic acid and converted into iron core. Figure 1D, E and narrow size distribution (Supporting Information Figure S2) indicate the monondispersed nanocapsules were obtained successfully with an average length of 420 ± 20 nm and width of 110 nm ±10 nm. These multifunctional magnetic "eyes" consist of an iron nanocylinder 85 nm long and 60 nm in diameter, an ellipsoidal silica shell ∼18 nm thick, and an outer coating of polyeletrolytes ∼8 nm thick. These components can be distinguished especially in Figure 1C and E due to the different electron penetrability between the iron core, silica shell, and polyelectrolytes. In addition, the size of the partially dissolved iron cores can be controlled by varying the etching time in oxalic acid.[43]

The crystal structure and composition of these nanocapsules were characterized by powder X-ray diffraction (XRD). The magnetic core is shown as α-Fe according to the data of JCPDS card no. 06-0696. The XRD of surface passivized iron nanoparticles shows highly stable over six months in the air at room temperature (Figure 2A, B). After PLL and AL coating and DOX/Gd-DTPA loading, the iron nanoparticles are also highly stable in PBS solution over at least a month (Figure 2C, D).

In order to investigate whether the silica shell around the magnetic capsules was permeable to small molecules (e.g., DOX and Gd-DTPA) for drug encapsulation, the Barret−Joner−Halenda (BJH) method was used to characterize the pore size in the silica shell. The result indicates that the silica shell is mesoporous with a pore size distribution of 2.4 nm, which is large enough for small molecules to penetrate. The uniform mesoporous pore size (Figure S3, Supporting Information) along with magnetic core (Fe) are advantageous for drug delivery applications.

To provide a biocompatible pH-dependent shell coating around the nanocapsules, a PLL/AL polyelectrolyte multilayer was coated onto the surface using layer-by-layer deposition. Since the uncoated particles were negative charged (ζ-potential was −18.5 mV), the first layer of polyelectrolyte applied to the nanocapsules was positively charged PLL. Subsequently, AL and PLL were alternately adsorbed onto the nanocapsules by the electrostatic interaction between the amino groups of PLL and the carboxyl groups of AL. As shown in Figure 3, the ζ-potentials of the PLL/AL multilayer coated Fe@SiO_2 alternated from negative to positive as each successive layer was applied. After eight coating steps, the polyelectrolyte coating on the nanocapsules was an average of 8 nm thick (Figure 1D, E).

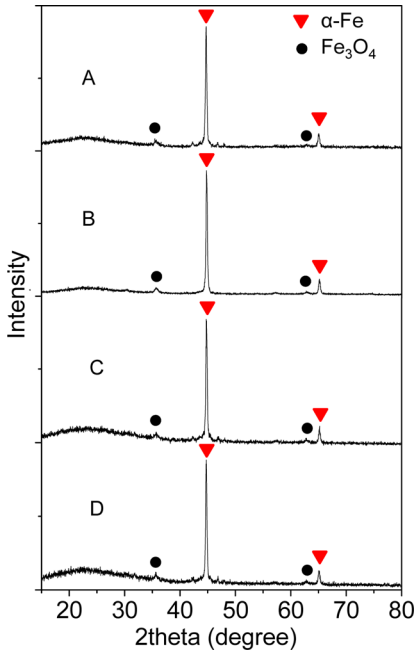

Figure 2. XRD pattern of (A) α-Fe@SiO_2, (B) α-Fe@SiO_2 in the air for 6 months, (C) (Fe/DOX/Gd-DTPA)@SiO_2@AL/PLL, (D) (Fe/DOX/Gd-DTPA)@SiO_2@AL/PLL in PBS buffer for a month.

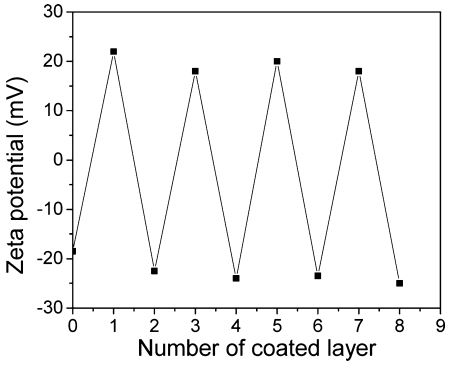

Figure 3. ζ-Potentials of the PLL/AL multilayer coated Fe@SiO_2 nanocapsules as a function of the layer number.

The FTIR spectrum in Figure 4 of poly-L-lysine and sodium alginate coated Fe@SiO_2 exhibited characteristic absorption bands of sodium alginate at 3445, 1614, 1417, and 1026 cm^{-1}, which are due to the stretching of −OH, −COO (asymmetric),

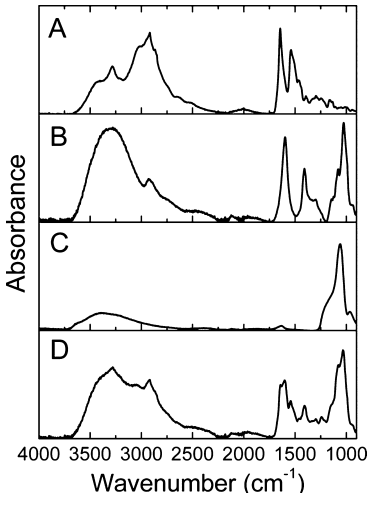

Figure 4. FTIR spectra of (A) poly-L-lysine, (B) sodium alginate, (C) Fe@SiO_2, and (D) poly-L-lysine and sodium alginate coated Fe@SiO_2.

dx.doi.org/10.1021/cm404168a | Chem. Mater. 2014, 26, 2105−2112

−COO (symmetric), and C−O−C, respectively. The FTIR spectrum also indicates the presence of poly-L-lysine on poly-L-lysine and sodium alginate coated Fe@SiO_2 nanoparticles showing peaks at 1620−1700 cm^{-1} that can be attributed to amide I (mainly CO group stretching mode) and the peak at 1534 cm^{-1} corresponds to amide II. The peaks for the CH_2 stretching modes of poly-L-lysine can be seen at 2936 cm^{-1}. Together with the alternating ζ-potential measurements (Figure 3), these FTIR measurements confirm the successful incorporation of PLL and AL on the outer Fe@SiO_2 nanocapsules.

DOX and Gd-DTPA were loaded into the PLL/AL-coated nanocapsules at pH 5, where the dissociation of PLL and AL allows the entrance of the DOX because ionization of carboxyl groups in the AL decreased greatly when the solution pH decreased from 7.4 to 5.0 (pK_a of sodium alginate 3.5 ± 0.05).[45] After encapsulation, however, the pH was increased from 5.0 to 7.4, trapping the drugs. At pH 7.4, both the carboxyl groups in AL and the amine groups in PLL are ionized (pK_a of sodium alginate 9.36 ± 0.08),[46] causing strong electrostatic attraction between PLL and AL which prevents material exchange between the inner particles and outer environment. pH-dependent interactions between the drug and capsule also influence the release rate. The presence of encapsulated DOX was confirmed by the fluorescence images of the (Fe/DOX/Gd-DTPA)@SiO_2@AL/PLL nanocapsules (Supporting Information Figure S4A), which show small well-dispersed fluorescent particles. To verify colloidal stability, dynamic light scattering was used to measure particle size based on particle diffusion rate under Brownian motion. The result, shown in Supporting Information Figure S4B, indicates that the drug-loaded nanocapsules a hydrodynamic size of 453 nm with minimal aggregation.

In order to clarify whether the DOX was encapsulated within the hollow cavities or retained only in the silica shell and polylectrolyte coating, we fabricated silica-coated iron nanoparticles with a solid core (by omitting the iron oxide etching stage) and applied the same protocols to load DOX/Gd-DTPA into these solid particles (Supporting Information Figure S5). The drug-loading of these nanoparticles with solid cores was only 2.5% w/w, compared to 13.5% (w/w) for the nanoeyes. This result suggests the majority of the drug is encapsulated in the cavity of the nanocapsules. To study the release rate at normal physiological pH and in acidic cancer environments, we measured the release rate in pH 7.4 PBS and 5.0, respectively. The cumulative release profile of doxorubicin from these nanocapsules is pH-dependent (Figure 5). The drug release is enhanced at pH 5.0 which is applicable for cancer therapy due to the low pH environment in tumors and within endosomes after internalization by cancer cells.[47] Based upon exponential fitting to the HPLC release curve, the release rate time constant was estimated to be ~28 days at pH 7.4, and 12.5 h at pH 5.0, respectively, which is shorter than the nanocapsules with thicker polymeric layers.[24] These results suggested that the release rate time constant is tunable depends on the layer thickness of polyelectrolytes coated on the nanocapsules. After 48 h, 82.5% encapsulated DOX in (Fe/DOX/Gd-DTPA)@SiO_2@AL/PLL was released at pH 5.0, while only 5.5% of encapsulated DOX was released at pH 7.4.

Cell viability tests indicate that the iron nanocore (Fe) (after removing silica coating with sodium hydroxide), empty silica nanocapsules (SiO_2), empty nanocapsules (Fe@SiO_2), and the PLL/AL multilayers coated nanocapsules (Fe@SiO_2@PLL/AL) show no significant toxicity up to a concentration of 1000 μg/mL (Figure 6A). To evaluate the feasibility of the DOX loaded (Fe/DOX/Gd-DTPA)@SiO_2@AL/PLL for the treatment of breast cancer, we examined the cytotoxic effect of the DOX loaded (Fe/DOX/Gd-DTPA)@SiO_2@AL/PLL on MCF-7 cell line. (Fe/DOX/Gd-DTPA)@SiO_2 and (Fe/DOX/Gd-DTPA)@SiO_2@AL/PLL nanoparticles were used to study cell growth inhibition in vitro. We expected that if the paricles released their contents rapidly before uptake (e.g., uncoated particles), the toxicity would be approximately the same as the free drug. Conversely, if the particles remained in the medium but did not release much of their contents (e.g., for

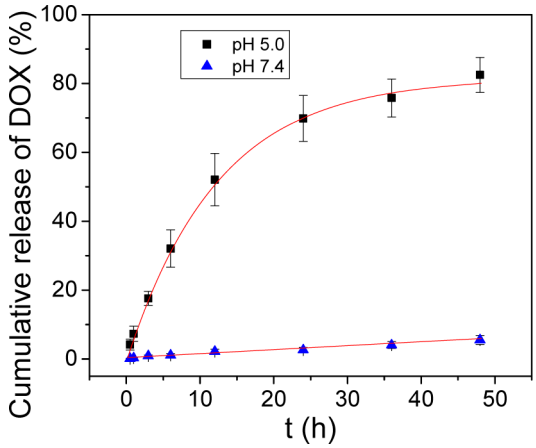

Figure 5. pH-triggered DOX release profile of DOX from (Fe/DOX/Gd-DTPA)@SiO_2@AL/PLL nanocapsules.

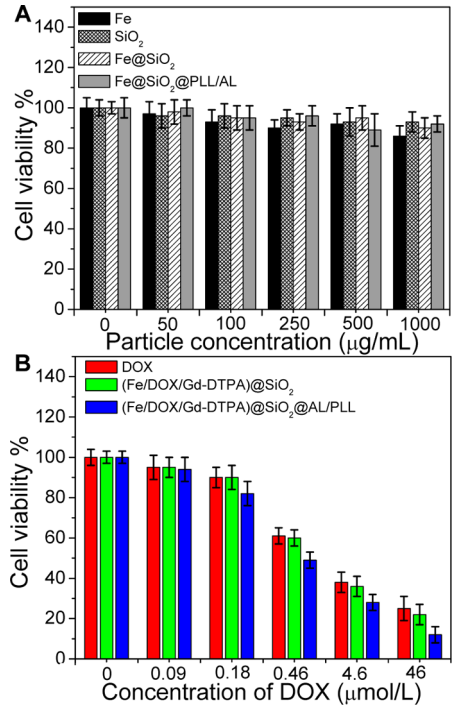

Figure 6. (A) Cytotoxicity test of iron core after removing silica coating (Fe), silica shell (SiO_2), silica coated iron nanocore (Fe@SiO_2), and alternating layers of PLL and AL coated magnetic nanocapsules (Fe@SiO_2@PLL/AL). (B) Cell viability of MCF-7 cells after incubating with different drug formulations at different concentrations for 48 h.

dx.doi.org/10.1021/cm404168a | Chem. Mater. 2014, 26, 2105−2112

coated nanocapsules at pH 7.4), the toxicity would be greatly reduced. However, if the particles were taken up and release in acidic organelles, the toxicity would be equal or greater than the free drug. The results shown in Figure 6B that cell viability decreases significantly when MCF-7 cells were treated with DOX-loaded Fe@SiO_2 and Fe@SiO_2@PLL/AL or free DOX at high DOX concentration. The uncoated particles did not have significantly different toxicity from free drug, which is consistent with rapid release into solution. Additionally, the Fe@SiO_2@PLL/AL nanocapsules showed higher cytotoxicity than nanocapsules without PLL/AL coating or free DOX at the same drug dose (0.09−46 μmol/L). Within this dose range, the increased toxicity of Fe/DOX/Gd-DTPA)@SiO_2@AL/PLL compared with (Fe/DOX/Gd-DTPA)@SiO_2 and free DOX is statistically significant ($p < 0.05$) for concentrations of 0.18 μmol/L and above. Although the increased toxicity for drug-loaded nanoparticles is modest, these in vitro studies do not include a mechanism to clear the drug. The corresponding in vivo doses will be different because of clearance from the circulation (e.g., free DOX has a circulation half-life of <5 min,[48] which depletes drug from uptake by cancer cells and increases doses to normal tissue). Nonetheless, the in vitro studies do show that DOX-loaded particles in cell culture release drug and are toxic to MCF-7 cancer cells.

The magnetic hysteresis curves for empty and drug-loaded nanoeyes are shown in Figure 7. The saturation magnetization

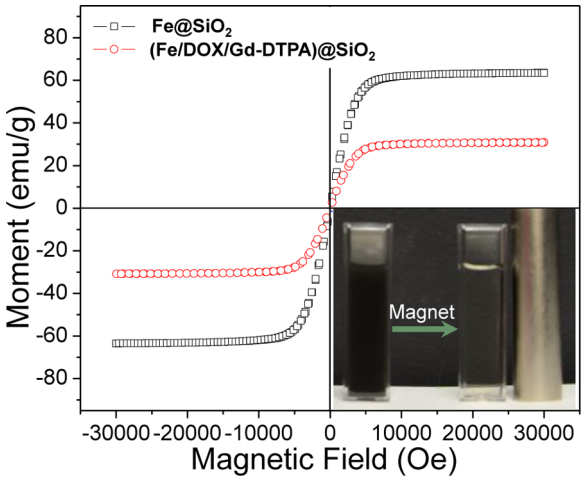

Figure 7. Magnetic hysteresis loop of Fe@SiO_2 and (Fe/DOX/Gd-DTPA)@SiO_2@AL/PLL.

of empty magnetic nanoeyes and DOX and Gd-DPTA encapsulated nanoeyes are 63.4 and 30.3 emu/g, respectively. ICP tests on these samples shows that the iron core comprises 31.1% and 15.3% of total mass in the Fe@SiO_2 and (Fe/DOX/Gd-DTPA)@SiO_2@AL/PLL, respectively. The normalized saturation magnetization calculated only by iron content in Fe@SiO_2 and (Fe/DOX/Gd-DTPA)@SiO_2@AL/PLL nanoparticles are 204 and 198 emu/g, respectively. These magnetization data are very close to reported saturation magnetization of α-Fe nanoparticles (212 emu/g),[16] which is much higher than that of nanocapsules with maghemite or magnetite nanocore.[43] In addition to greater magnetization, the coercivity of the magnetic nanoeyes with DOX and Gd-DTPA encapsulated nanoeyes is about 240 Oe.

The magnetic nanoeyes also potentially serve as T_1 and T_2-weighted MRI contrast agents due to the ferromagnetic α-Fe core and paramagnetic Gd-DTPA. In order to measure their relaxivities, different concentrations of magnetic nanoeyes with encapsulated DOX and Gd-DTPA were prepared in 1 wt % agarose gel and imaged with a 4.7 T MRI instrument. Figure 4 clearly shows the positive T_1 and negative T_2 contrast effects of the magnetic nanophosphors: the T_1-weighted images become brighter with increased particle concentration, while the T_2-weighted images become darker with increased particle concentration. The T_1 relaxivity coefficient (r_1) for the magnetic nanoeyes could also be calculated from the curve of $1/T_1$ vs concentration of gadolinium (Figure 8A). The data

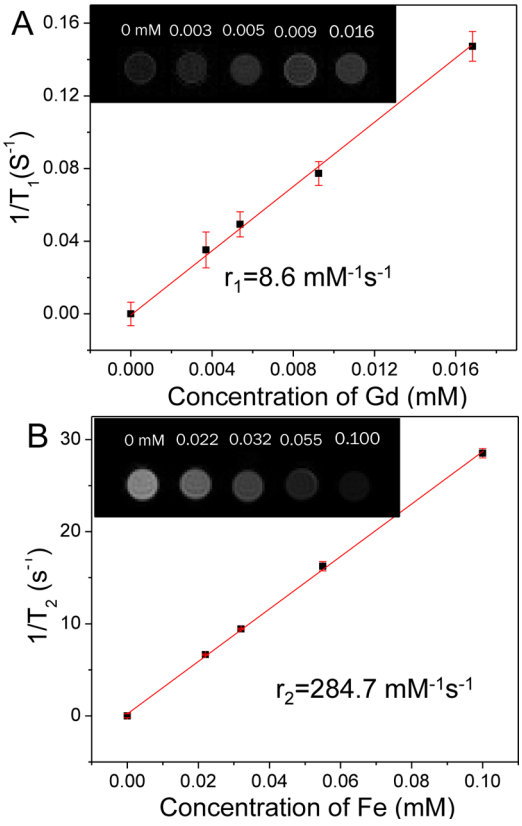

Figure 8. T_1 (A) and T_2 (B)-weighted images of magnetic at echo time of 4 ms.

shows that r_1 is 8.6 (mM Gd)$^{-1}$ s^{-1} which is higher than the relaxivity of free Gd-DTPA (5.5 mM^{-1} s^{-1}, measured in the same instrument and gel, at 4.7 T). The increased relaxivity is likely due to the relaxivity contribution from iron core and interactions between the Gd-DTPA and polyelectrolytes; the overall relaxivity is 2.3 (mM Fe +Gd)$^{-1}$ s^{-1}. Additionally, the calculated r_2 is 285 (mM Fe)$^{-1}$ s^{-1}, which is much larger than FDA-approved iron oxide nanoparticle contrast agents such as Ferumoxtran (Resovist, 65 mM^{-1} s^{-1}), cross-linked iron oxide particle (CLIO-Tat, 62 mM^{-1} s^{-1}), and water-soluble iron oxide (WSIO, 78 mM^{-1}s^{-1}).[49−51]

To evaluate the stability of encapsulated Gd-DTPA in (Fe/DOX/Gd-DTPA)@SiO_2@AL/PLL nanocapsules, the release behavior of encapsulated Gd-DTPA was sudied at pH 7.4 PBS and 5.0, respectively. The total loading of Gd-DTPA was 11.5% (w/w). The cumulative release profile of Gd-DTPA from these nanocapsules is pH-dependent (Supporting Information Figure S6). Interestingly, a slower release rate of Gd-DTPA was found compared with DOX (e.g., after 24 h at pH 5.0, 48% of the Gd-

dx.doi.org/10.1021/cm404168a | Chem. Mater. 2014, 26, 2105−2112

DTPA was released compared with 82.5% of the DOX), which could be due to stronger interactions between Gd-DTPA and the carboxylic groups within polyelectrolytes. Additionally, no significant release (4.5%) of Gd-DTPA was observed at 7.4 after 48 h (Supporting Information Figure S6). These results suggest the Gd-DTPA is stable in (Fe/DOX/Gd-DTPA)@SiO_2@AL/PLL nanocapsules at physiological conditions.

■ CONCLUSIONS

High magnetization magnetic carriers for pH controlled drug release and dual MRI contrast agents were successfully prepared. The mesoporous silica coating on magnetic core plays a critical role to prevent iron nanoparticle aggregation during hydrogen reduction of α-Fe_2O_3 and for drug encapsulation. The DOX release rate is controlled by pH due to the biocompatible multilayers of polyelectrolytes on the surface of magnetic nanocarriers. Encapsulation a T_1-weighted MRI contrast agent (Gd-DTPA) is advantageous as it allows multimodal MRI tracking of the magnetic nanoeyes and the encapsulated drug. We expect that such bifunctional nanocarriers, combining the advantages of magnetic drug delivery, controlled drug release, and MRI contrast, will find applications in anticancer therapy. Furthermore, the hollow structure in the magnetic nanoeyes allows high drug loading efficiency. Our synthesis technique is attractive because multifunctional particles can be made by coating the core templates with multiple layers of materials each with controlled thickness. Future work will study the magnetic field directed drug delivery and the drug release in vivo. The dual MRI images of the drug encapsulated nanoeyes will be used to track the location of the encapsulated drug.

■ ASSOCIATED CONTENT

Supporting Information

Additional details of characterizations. This material is available free of charge via the Internet at http://pubs.acs.org.

■ AUTHOR INFORMATION

Corresponding Author

*Tel: +1-864-656-1726. E-mail: janker@clemson.edu.

Present Address

[⊥](H.C.) Ocean NanoTech, LLC, 7964 Arjons Drive, Suite G San Diego, CA 92126, United States

Author Contributions

[#]H.C. and D.S. contributed equally.

Notes

The authors declare no competing financial interest.

■ ACKNOWLEDGMENTS

This research was supported in part by National Science Foundation (NSF) CAREER award CHE1255535 to H.C. and J.N.A., an NSF award DMR-0077321 to D.S. and S.-J.H., an NSF award CMMI-1100684 to B.Q. and O.T.M., and an NSF award CMMI-1130636 to T.C. Electron microscopy images were acquired at the Clemson University Electron Microscope Facility and use of this facility was funded by The Center of Biomaterials for Tissue Regeneration (CBTR) funded under National Institutes of Health (NIH) grants 5P20RR021949 and 8P20GM103444.

■ REFERENCES

(1) Morelli, D.; Ménard, S.; Colnaghi, M. I; Balsari, A. *Cancer Res.* **1996**, *56*, 2082−2085.

(2) Von Hoff, D. D.; Layard, M. W.; Basa, P.; Davis, J. H. L.; Von Hoff, A. L.; Rozencweig, M.; Muggia, F. M. *Ann. Intern. Med.* **1979**, *91*, 710−717.

(3) Dobson, J. *Drug Dev. Res.* **2006**, *67*, 55−60.

(4) Alexis, F.; Anker, J. N. *Ther. Delivery* **2014**, *5*, 97−100.

(5) Moore, T.; Chen, H.; Morrison, R.; Wang, F.; Anker, J. N; Alexis, F. *Mol. Pharmaceutics* **2013**, *11*, 24−39.

(6) Alexis, F.; Pridgen, E.; Langer, R.; Farokhzad, O. In *Nanoparticle Technologies for Cancer Therapy*; Schäfer-Korting, M., Ed.; Springer: Berlin Heidelberg, 2010; Vol. *197*, pp 55−86.

(7) Wang, A. Z.; Bagalkot, V.; Vasilliou, C. C.; Gu, F.; Alexis, F.; Zhang, L.; Shaikh, M.; Yuet, K.; Cima, M. J.; Langer, R.; Kantoff, P. W.; Bander, N. H.; Jon, S.; Farokhzad, O. C. *ChemMedChem* **2008**, *3*, 1311−1315.

(8) Lee, J. E.; Lee, N.; Kim, H.; Kim, J.; Choi, S. H.; Kim, J. H.; Kim, T.; Song, I. C.; Park, S. P.; Moon, W. K; Hyeon, T. *J. Am. Chem. Soc.* **2009**, *132*, 552−557.

(9) Wang, D.; He, J.; Rosenzweig, N.; Rosenzweig, Z. *Nano Lett.* **2004**, *4*, 409−413.

(10) Anker, J. N; Kopelman, R. *Appl. Phys. Lett.* **2003**, *82*, 1102.

(11) Lu, H.; Yi, G.; Zhao, S.; Chen, D.; Guo, L. H; Cheng, J. *J. Mater. Chem.* **2004**, *14*, 1336−1341.

(12) Johannsen, M.; Gneveckow, U.; Eckelt, L.; Feussner, A.; Waldöfner, N.; Scholz, R.; Deger, S.; Wust, P.; Loening, S.; Jordan, A. *Int. J. Hyperthermia* **2005**, *21*, 637−647.

(13) Feng, J.; Shan, G.; Maquieira, A.; Koivunen, M. E.; Guo, B.; Hammock, B. D; Kennedy, I. M. *Anal. Chem.* **2003**, *75*, 5282−5286.

(14) Yu, M. K.; Jeong, Y. Y.; Park, J.; Park, S.; Kim, J. W.; Min, J. J.; Kim, K.; Jon, S. *Angew. Chem., Int. Ed.* **2008**, *47*, 5362−5365.

(15) Ma, H. L.; Xu, Y. F.; Qi, X. R.; Maitani, Y.; Nagai, T. *Int. J. Pharm.* **2008**, *354*, 217−226.

(16) Nikitenko, S. I.; Koltypin, Y.; Palchik, O.; Felner, I.; Xu, X. N; Gedanken, A. *Angew. Chem., Int. Ed.* **2001**, *40*, 4447−4449.

(17) Hadjipanayis, C. G.; Bonder, M. J.; Balakrishnan, S.; Wang, X.; Mao, H.; Hadjipanayis, G. C. *Small* **2008**, *4*, 1925−1929.

(18) Peng, S.; Wang, C.; Xie, J.; Sun, S. *J. Am. Chem. Soc.* **2006**, *128*, 10676−10677.

(19) Khurshid, H.; Hadjipanayis, C. G.; Chen, H.; Li, W.; Mao, H.; Machaidze, R.; Tzitzios, V.; Hadjipanayis, G. C. *J. Magn. Magn. Mater.* **2013**, *331*, 17−20.

(20) Chen, Y.; Chen, H.; Guo, L.; He, Q.; Chen, F.; Zhou, J.; Feng, J.; Shi, J. *ACS Nano* **2009**, *4*, 529−539.

(21) Esser-Kahn, A. P.; Odom, S. A.; Sottos, N. R.; White, S. R; Moore, J. S. *Macromolecules* **2011**, *44*, 5539−5553.

(22) De Geest, B. G.; Sanders, N. N.; Sukhorukov, G. B.; Demeester, J.; De Smedt, S. C. *Chem. Soc. Rev.* **2007**, *36*, 636−649.

(23) Mendelsohn, J. D.; Barrett, C. J.; Chan, V. V.; Pal, A. J.; Mayes, A. M; Rubner, M. F. *Langmuir* **2000**, *16*, 5017−5023.

(24) Chen, H.; Moore, T.; Qi, B.; Colvin, D. C.; Jelen, E. K.; Hitchcock, D. A.; He, J.; Mefford, O. T.; Gore, J. C.; Alexis, F.; Anker, J. N. *ACS Nano* **2013**, *7*, 1178−1187.

(25) Wu, W.; Liu, W.; Wang, S.; Liu, Y. In *Drug Controlled Release of Novel Alginate/Poly-L-arginine Microcapsules*; Peng, Y., Weng, X., Eds.; Springer: Berlin Heidelberg, 2008; Vol. *19*, pp 26−28.

(26) Orive, G.; Tam, S. K.; Pedraz, J. L; Hallé, J.-P. *Biomaterials* **2006**, *27*, 3691−3700.

(27) Decher, G. *Science* **1997**, *277*, 1232−1237.

(28) Caruso, F.; Caruso, R. A; Möhwald, H. *Science* **1998**, *282*, 1111−1114.

(29) Hu, S.-H.; Tsai, C.-H.; Liao, C.-F.; Liu, D.-M; Chen, S.-Y. *Langmuir* **2008**, *24*, 11811−11818.

(30) Angelatos, A. S.; Johnston, A. P. R.; Wang, Y.; Caruso, F. *Langmuir* **2007**, *23*, 4554−4562.

(31) Khapli, S.; Kim, J. R.; Montclare, J. K.; Levicky, R.; Porfiri, M.; Sofou, S. *Langmuir* **2009**, *25*, 9728−9733.

(32) Becker, A. L.; Zelikin, A. N.; Johnston, A. P. R.; Caruso, F. *Langmuir* **2009**, *25*, 14079−14085.
(33) Gai, S.; Yang, P.; Li, C.; Wang, W.; Dai, Y.; Niu, N.; Lin, J. *Adv. Funct. Mater.* **2010**, *20*, 1166−1172.
(34) Brunauer, S.; Emmett, P. H; Teller, E. *J. Am. Chem. Soc.* **1938**, *60*, 309−319.
(35) Champion, J. A; Mitragotri, S. *Proc. Natl. Acad. Sci. U.S.A.* **2006**, *103*, 4930−4934.
(36) Huang, X.; Li, L.; Liu, T.; Hao, N.; Liu, H.; Chen, D.; Tang, F. *ACS Nano* **2011**, *5*, 5390−5399.
(37) Decuzzi, P.; Pasqualini, R.; Arap, W.; Ferrari, M. *Pharm. Res.* **2009**, *26*, 235−243.
(38) Alexis, F.; Pridgen, E.; Molnar, L. K; Farokhzad, O. C. *Mol. Pharmaceutics* **2008**, *5*, 505−515.
(39) Ishikawa, T.; Matijevic, E. *Langmuir* **1988**, *4*, 26−31.
(40) Ozaki, M.; Kratohvil, S.; Matijević, E. *J. Colloid Interface Sci.* **1984**, *102*, 146−151.
(41) Lou, X. W; Archer, L. A. *Adv. Mater.* **2008**, *20*, 1853−1858.
(42) Chen, J. S.; Chen, C.; Liu, J.; Xu, R.; Qiao, S. Z; Lou, X. W. *Chem. Commun.* **2011**, *47*, 2631−2633.
(43) Chen, H.; Colvin, D. C.; Qi, B.; Moore, T.; He, J.; Mefford, O. T.; Alexis, F.; Gore, J. C; Anker, J. N. *J. Mater. Chem.* **2012**, *22*, 12802−12809.
(44) Gai, S.; Yang, P.; Hao, J.; Wang, W.; Niu, N.; He, F.; Wang, D.; Lin, J. *Microporous Mesoporous Mater.* **2010**, *131*, 128−135.
(45) Mu, B.; Liu, P.; Li, X.; Du, P.; Dong, Y.; Wang, Y. *Mol. Pharmaceutics* **2011**, *9*, 91−101.
(46) Burke, S. E; Barrett, C. J. *Biomacromolecules* **2003**, *4*, 1773−1783.
(47) Schmaljohann, D. *Adv. Drug Delivery Rev.* **2006**, *58*, 1655−1670.
(48) Gabizon, A.; Shmeeda, H.; Barenholz, Y. *Clin. Pharmacokinet.* **2003**, *42*, 419−436.
(49) Wang, Y.; Hussain, S.; Krestin, G. *Eur. J. Radiol.* **2001**, *11*, 2319−2331.
(50) Josephson, L.; Tung, C.; Moore, A.; Weissleder, R. *Bioconjugate Chem.* **1999**, *10*, 186−191.
(51) Jun, Y.; Huh, Y.; Choi, J.; Lee, J.; Song, H.; Kim, K.; Yoon, S.; Kim, K.; Shin, J.; Suh, J.; Cheon, J. *J. Am. Chem. Soc.* **2005**, *127*, 5732−5733.